The Gauge Theory Bootstrap: Predicting pion dynamics from QCD

Yifei He¹, Martin Kruczenski² *

¹ Laboratoire de Physique de l'École Normale Supérieure, ENS, Université PSL, CNRS, Sorbonne Université, Université Paris Cité, F-75005 Paris, France
² Department of Physics and Astronomy and PQSEI[†], Purdue University, West Lafavette, IN 47907, USA.

May 27, 2025

Abstract

The Gauge Theory Bootstrap [1–3] computes the strongly coupled pion dynamics by considering the most general scattering matrix, form factors and spectral densities and matching them with perturbative QCD at high energy and with weakly coupled pions at low energy. In this work, we show that further constraints on the spectral densities significantly reduce the possible solutions to a small set of qualitatively similar ones. Quantitatively, the precise solution is controlled by the asymptotic value of the form factors and SVZ sum rules. We also introduce an iterative procedure that, starting from a generic feasible point, converges to a unique solution parameterized by the UV input. For the converged solution we compute masses and widths of resonances that appear, scattering lengths and effective ranges of partial waves, low energy coefficients in the effective action. Additionally, we use these results to discuss the thermodynamics of a pion gas including pair correlations of pions with same and opposite charge.

^{*}E-mail: yifei.he@ens.fr, markru@purdue.edu.

[†]Purdue Quantum Science and Engineering Institute

Contents

1	Motivation and summary				
2	New ingredients to the GTB procedure 2.1 Low energy spectral density	4 5 7			
3	Convergence of the solution 3.1 Test by computing the pion coupling λ	9 9 10 11			
4	Detailed study of a converged solution 4.1 Low energy parameters and one-loop χ_{PT} amplitude	12 14 15			
5	Dependence on the input parameters 5.1 Form factor asymptotics	16 16 17			
6	Thermodynamics of a dilute gas of pions, second virial coefficients and density of pion pairs				
7	Conclusions				
8	Acknowledgements				
\mathbf{A}	Chiral Lagrangian and one-loop amplitude				
В	Parameterization of the spectral density				
\mathbf{C}	Finite energy sum rules up to 3-loop				

1 Motivation and summary

In asymptotically free gauge theories, the UV is understood in perturbation theory, and the IR is understood as a weakly coupled theory of pions determined by symmetries and the mass m_{π} and coupling f_{π} of the pion. In the intermediate energy region both descriptions are strongly coupled and the dynamics is difficult to solve. That region has a rich dynamics known from phenomenological analysis of experiments [4–11] and from lattice simulations [12].

In [1–3] we proposed the Gauge Theory Bootstrap (GTB), a method to understand this region from a purely theoretical point of view. The idea is to write the most general S-matrix, form factors and current spectral densities that satisfy basic physical properties and add more and more constraints based on matching of the physics to the known UV and IR. In that way we expect to converge to a unique solution parameterized by the UV and IR properties. In this paper we get much closer to this main goal by adding further IR constraints on the spectral density that greatly reduce the space of solutions and, further, by creating an iterative procedure that pushes the constraints towards saturation and converges to a unique solution. Instead of using a functional to map out the space of solutions, and extract extremal amplitudes as we did in previous work, we can remove the functional and allow the program to choose an arbitrary feasible point and then use this iterative procedure to converge to a solution. This differs from the standard S-matrix bootstrap procedure that uses kinematic constraints to put bounds on theory parameters, instead we introduce dynamical information¹ from the UV and IR to compute the S-matrix. In that way, we perhaps go back to the original bootstrap philosophy of the 1960's [13, 14] but augmented with the microscopic dynamical information that was not known at that time. In that work [13, 14] the dynamical information was the idea of self-consistency, or hadron democracy: for example the ρ meson gave rise to an attractive potential between pions which in turn gave rise to a resonance, the ρ meson itself (see for example [15, 16]). Although interesting, such ideas did not match the experimental results and were superseded by QCD. In the recent bootstrap revival [17–20], powerful numerical methods were used to put bounds on couplings and other parameters of generic quantum field theories, including the effective field theory of pions [21–28]. This also extended to form factors and spectral densities (mostly in 2d theories) [29–33]. However it is clear that general kinematical constraints still allow an enormous number of theories and that dynamical information, here provided by QCD, is necessary to identify the correct theory. In that way, without using experimental input, we can predict and *compute* low energy constants,

¹We are grateful to A. Vainshtein for emphasizing this point.

partial waves, form factors, resonance spectrum, etc. For example in the recent work [34] this method was used as a tool to compute the g-2 factor contribution from hadrons. Notice also that the only assumption on the spectrum is that there are no bound states. The number of resonances together with their masses and widths are results of the computation based on the UV input from pQCD and matching with low energy pions.

One caveat that became apparent due to this improved procedure is that, at the moment, the results depends on having accurate values of the form factors at high (but not asymptotically high) energy ($\sqrt{s} \sim 2 \,\mathrm{GeV}$). At that energy calculations of the Brodsky-Lepage [35] type give the form factors up to a factor of order one. Therefore we allow for a range of values starting from the minimum that the constraints allow. We discuss this later in the paper. On the plus side, the asymptotic form factors is the only place where f_{π} is used and as we just mentioned, we allow for a range of values meaning that the precise value of f_{π} is not really used. Therefore, f_{π} when interpreted as a low-energy coupling is an outcome of our computation.

2 New ingredients to the GTB procedure

The procedure we use in this paper is basically the same as described in previous work and we refer the interested reader to [1–3] for necessary details and main notation². In this section we discuss two crucial new additions to the GTB procedure. First we introduce, from χ_{PT} , constraints on the low energy kinematic (i.e. from the free pion Lagrangian) behavior of the spectral densities using a parameterization that we discuss in the appendix. Second, and perhaps the most importantly, we devise an iterative procedure that starts from an arbitrary feasible point and converges to a unique solution (after fixing the UV and IR information). We now discuss those new ingredients in detail as well as the input from the asymptotic form factors. Once more, the only numerical input to the GTB procedure are the values of m_{π} that sets the units, f_{π} that is used in the asymptotic form factors, α_s , $N_c = 3$, $N_f = 2$ and m_q from the gauge theory to compute the SVZ sum rules [37–39]. At the moment, however, all pQCD calculations are done with $m_q = 0$ assuming $m_q \ll \Lambda_{QCD}$. Therefore m_q only appears as an overall factor in the S0 sum rule. Presumably m_q should be computed by consistency in future work. The fact that f_{π} does not appear in the low energy matching, and only in the asymptotic form factors is discussed around eq.(5.15).

²See [36] for an alternative numerical implementation

2.1 Low energy spectral density

A major role in the Gauge Theory Bootstrap is played by the currents³, a set of QCD operators chosen to match the quantum numbers of the different partial waves. In this and previous papers we consider the following operators for $N_f = 2$

$$j_S = m_q(\bar{u}u + \bar{d}d) = \frac{1}{2}m_\pi^2\pi^a\pi^a + \mathcal{O}(\pi^4)$$
 (2.1a)

$$j_V = \frac{1}{2} (\bar{u}\gamma^{\mu}u - \bar{d}\gamma^{\mu}d)\Delta_{\mu} = \epsilon^{abc}\pi^b\partial_{\Delta}\pi^c + \mathcal{O}(\pi^4)$$
 (2.1b)

$$j_T = T^{\mu\nu} \Delta_{\mu} \Delta_{\nu} \tag{2.1c}$$

written both from QCD and from the free pion Lagrangian. Here $T^{\mu\nu}$ is the energy momentum tensor (either in QCD or in terms of pions) and $\Delta_{\mu} = (0, 1, i, 0)$ is a (complex) light-like vector $\Delta^2 = 0$ with components in the (x, y) plane. In general, currents, can be identified at low energy up to a normalization constant, however, for these three, the normalization is known. Using the free pion Lagrangian, namely kinematically, one can compute the spectral densities at low energy [40]:

$$\rho_0^0(s) \simeq \frac{m_\pi^4}{(2\pi)^4} \frac{3}{16\pi} \left(1 - \frac{4m_\pi^2}{s}\right)^{\frac{1}{2}}$$
(2.2a)

$$\rho_1^1(s) \simeq \frac{1}{(2\pi)^4} \frac{s}{24\pi} \left(1 - \frac{4m_\pi^2}{s}\right)^{\frac{3}{2}}$$
(2.2b)

$$\rho_2^0(s) \simeq \frac{1}{(2\pi)^4} \frac{s^2}{160\pi} \left(1 - \frac{4m_\pi^2}{s}\right)^{\frac{5}{2}}$$
(2.2c)

In appendix B we describe a parameterization of the spectral densities that takes into account this behavior. This is the first addition to the procedure and plays a crucial role because the spectral density is now also constrained in the IR and not only in the UV (by the SVZ sum rules).

2.2 Iterative "Watsonian" procedure

An important ingredient of any bootstrap program are positivity constraints associated with the positivity of the norm in Quantum Mechanics, for example in the Gauge Theory Bootstrap we use (2.7) below. If a large enough matrix, with many

³It is customary to call QCD operators currents whether they are actual currents or not. Of course these operators play an important role in most studies of QCD, not just here.

pion states and QCD operators included is considered, we expect such matrix of state overlaps to saturate the positivity condition since scattering is unitary and QCD operators acting on the vacuum should be representable as linear combinations of pion states giving rise to zero modes or null states. In (2.7) below, where only two pion states are considered, this saturation should certainly be exact below the four pion threshold and approximately above. In general, we adopt the philosphy of always look for saturation of the constraints and, if that is not possible to further add pion states and QCD operators to the matrix. Once a matrix such as (2.7) is chosen, to achieve the desired saturation, we now introduce an iterative procedure that leads to a particular solution to the GTB constraints.

Iterative procedures in the S-matrix bootstrap were introduced initially in [41] to get closer to the boundary of the allowed space. The main idea is that, denoting the bootstrap variables as x_j , and given a constraint $\Phi_A(x_j) \leq 0$, after finding a solution $x_j = \bar{x}_j$, we can improve the solution by maximizing again in the direction of the gradient of the constraint. The unitarity constraint reads

$$(\operatorname{Re}h_{\ell}^{I}(s))^{2} + (\operatorname{Im}h_{\ell}^{I}(s))^{2} - 2\operatorname{Im}h_{\ell}^{I}(s) \leq 0, \quad s > 4m_{\pi}^{2}, \ \forall \ I, \ell$$
 (2.3)

where $h_{\ell}^{I}(s)$ is the normalized partial wave where

$$S_{\ell}^{I}(s) = 1 + ih_{\ell}^{I}(s) = \eta_{\ell}^{I}(s)e^{2i\delta_{\ell}^{I}(s)}$$
 (2.4)

with δ_{ℓ}^{I} the usual phase shift. It is known, qualitatively, that pion scattering tends to saturate unitarity even at energies larger than the four pion threshold.⁴ If we want to approach further the unitarity saturation region, the new functional to maximize, for the next iteration, is

$$\mathcal{F} = \int ds \sum_{\ell,I} \operatorname{Re}h_{\ell}^{I}(s) \big|_{old} \operatorname{Re}h_{\ell}^{I}(s) \big|_{new} + \operatorname{Im}h_{\ell}^{I}(s) \big|_{old} \operatorname{Im}h_{\ell}^{I}(s) \big|_{new} - \operatorname{Im}h_{\ell}^{I}(s) \big|_{new}$$
(2.5)

where old are the values from the previous iteration, and new are the values in the maximization that is being performed. In the case of two dimensions it was very successful in converging to the desired solutions. One might expect that the same happens here. And although this is true, once we include form factors and spectral densities in the bootstrap, Watson theorem provides a new natural iterative functional for our purpose. Watson theorem establishes that, when unitarity is saturated, the phase of the form factors agrees with the phase shift of the corresponding

⁴at higher energy we could incorporate some method of particle production such as was done in [42,43] or via resonance decay as suggested in [3]

partial wave. The procedure then replaces the phase of the previous (old) partial wave by the phase of the previous (old) form factor when computing the functional, i.e., in (2.5) we replace:

$$h_{\ell}^{I}(s)\big|_{old} \to \left(|h_{\ell}^{I}(s)| \frac{F_{\ell}^{I}(s)}{|F_{\ell}^{I}(s)|} \right) \Big|_{old}$$
 (2.6)

Namely instead of just using the old partial wave to determine the functional, we use its modulus and replace its phase by the phase of the form factor. Such iteration will tend to converge to unitarity saturation while matching the phase of the form factor with the phase shift. From a physical point of view, the UV information incorporated into the form factors and spectral densities is conveyed to the phase shifts and partial waves. At the same time the crossing and unitarity constraints on the partial waves feed back to the form factors. More precisely, following the form factor bootstrap [29,30] we introduce a 3×3 matrix of scalar products:

$$\frac{\langle \text{in}|_{P',\ell}}{\langle \text{out}|_{P',\ell}} \quad \begin{cases} |\text{out}\rangle_{P,\ell} & \mathcal{O}_{\ell,P}|0\rangle \\ S_{\ell}^*(s) & \mathcal{F}_{\ell} \\ \mathcal{F}_{\ell}^* & \mathcal{F}_{\ell} & \rho_{\ell}(s) \end{cases} \succeq 0, \quad \forall I, \ell, \ s > 4m_{\pi}^2, \tag{2.7}$$

where we removed an overall factor $\delta^4(P-P')$, namely the identity in the center of mass variable. The in- and out- states are two pion states and $\mathcal{O}_{\ell,P}$ is an integrated current. The elements of the matrix are the scattering matrix S_ℓ^I , the form factors \mathcal{F}_ℓ^I and the spectral density ρ_ℓ^I . When unitarity is saturated and the phase shift is equal to the phase of the form factor (Watson's theorem) this matrix has two zero eigenvalues. That means that two linear combinations of the states vanish. One simply means that the in and out states are the same (up to a phase) if there is no particle production. The other, interestingly, means that we have a way to write $\mathcal{O}_{\ell,P}|0\rangle$ as a two pion state. So, from a physical perspective, one can understand the Watsonian iteration as a way to write pQCD states (currents acting on vacuum) in terms of pion states and vice versa.

2.3 Asymptotic form factors

This new improved procedure highlights the need for more precise high energy inputs. This is not a problem for the SVZ sum rules [37–39] but it is a problem for the form factors. At high energy, the pion is highly boosted but in the transverse directions it has the same size given by its radius $R_{\pi} \sim \frac{1}{f_{\pi}}$. The probability of a probing

particle hitting a quark is inversely proportional to the transverse area. That is the reason that f_{π} appears in the asymptotic formulas. More technically, the parton distribution functions are required, a low energy information. At high energy the results of Brodsky-Lepage [3, 35, 44, 45] allows us to determine form factors as

$$|F_1^1(s)| \simeq \frac{16\pi\alpha_s f_\pi^2}{s} \tag{2.8a}$$

$$|F_2^0(s)| \simeq \frac{48\pi\alpha_s f_\pi^2}{s}$$
 (2.8b)

The scalar form factor was crudely estimated in [3] to be $|F_0^0(s)| \sim \frac{1}{s} \ln \left(\frac{s}{m_\pi^2}\right)$. At an energy $s_0 \sim 2 \text{GeV}$ these formulas are not quite valid. For example it has been argued that the P1 form factor changes by a factor of up to 3 [46]. So we define χ_ℓ^I , three rescaling factors of order one and require:

$$|F_0^0(s > s_0)| \le \chi_0^0 \frac{m_\pi^4}{s} \ln\left(\frac{s}{m_\pi^2}\right)$$
 (2.9a)

$$|F_1^1(s > s_0)| \le \chi_1^1 \frac{16\pi\alpha_s f_\pi^2}{s}$$
 (2.9b)

$$|F_2^0(s > s_0)| \le \chi_2^0 \frac{48\pi\alpha_s f_\pi^2}{s}$$
 (2.9c)

where in the scalar case we just chose the factor m_{π}^4 from units. If we choose any of these factors χ_{ℓ}^I to be one, the problem becomes unfeasible reflecting the fact that at s_0 we are not in the fully asymptotic region yet. Most plots in this paper are done with the values

$$\chi_0^0 = 8, \quad \chi_1^1 = 2.2, \quad \chi_2^0 = 9,$$
(2.10)

which are close to the minimum allowed values. The partial waves and form factors seems to agree reasonable well with the experimental results but this should not be taken as a strong prediction of the procedure. Later in section 5.1 we show how the solution changes if we change these values over a range (see figs. 8, 9, 10, 11). We emphasize that we are not just computing masses and widths of resonances but the whole amplitude and form factors as analytic functions. We do not assume how many resonances appear in each channel or any other qualitative information, so the overall picture is a result of the calculation. Also, notice again that this is the only place where the value of f_{π} enters.

3 Convergence of the solution

To test this new improved procedure, we fix the asymptotic (high energy) form factors and sum rules and then maximize and minimize a given physical quantity. The range of values should be relatively small and the partial waves associated with the maximum and minimum should be qualitatively similar. Furthermore, if we apply the iterative procedure to those initial solutions, or to any other arbitrary solution, the procedure should converge to a certain result. The values of the physical quantities for the given UV/IR input will be estimated by the values after convergence.

3.1 Test by computing the pion coupling λ

It is customary to define the coupling λ as the π^0 scattering amplitude at the symmetric point:

$$\lambda = \frac{1}{32\pi} \left. \mathcal{M}(\pi^0 \pi^0 \to \pi^0 \pi^0) \right|_{s=t=u=\frac{4}{3}m_\pi^2} = \frac{3\pi}{4} A\left(\frac{4}{3}m_\pi^2, \frac{4}{3}m_\pi^2, \frac{4}{3}m_\pi^2\right)$$
(3.11)

which is bounded from above and below from analycitity, crossing and unitarity: $-8.02 \le \lambda \le 2.661$ [19,47–51]. For low energy pions it is approximately (tree level amplitude)

$$\lambda \simeq \frac{m_{\pi}^2}{32\pi f_{\pi}^2} \simeq 0.023$$
 (3.12)

which, as we mentioned in [2], is a simple way to argue that the theory of pions is weakly coupled at low energy. In this work the low and high energy constraints severely restrict the values of λ . Given a set of input parameters, we maximize and minimize λ obtaining an initial spread $0.01 \lesssim \lambda \lesssim 0.022$. For the maximum and minimum, we plot the partial waves⁵ in six channels in fig.2 and see that they are qualitatively similar, except in the isospin I = 2 channels (S2 and D2) and the spin 3 (F1) channel, a fact that can be understood due to the lack of high energy input in those channels. This tells us that the space of solutions is indeed tightly controlled by the asymptotics as we can also see by changing the asymptotic values in sec.5. After that, we take the solutions associated with the maximum and the minimum and apply the iterative procedure of section 2.2. In figure 1 we show the convergence of the values of λ to a definite one, whether we start from the maximum λ , from the minimum or from a feasible point chosen by the optimizer (using no functional⁶).

⁵In all cases we always do one initial Watsonian iteration to smoothen out the functions.

⁶Technically the minimizer program is required to minimize an $\mathcal{F}=0$ functional

So, the final converged value of $\lambda=0.02$ we take as the computed value of λ for these values of the UV/IR input. The main thing we see, is that the existence of resonances in the S0, P1 and D0 channels is a generic result of the procedure that was not input in any way. This is mostly due to the SVZ sum rules combined with the asymptotic behavior of the form factors.

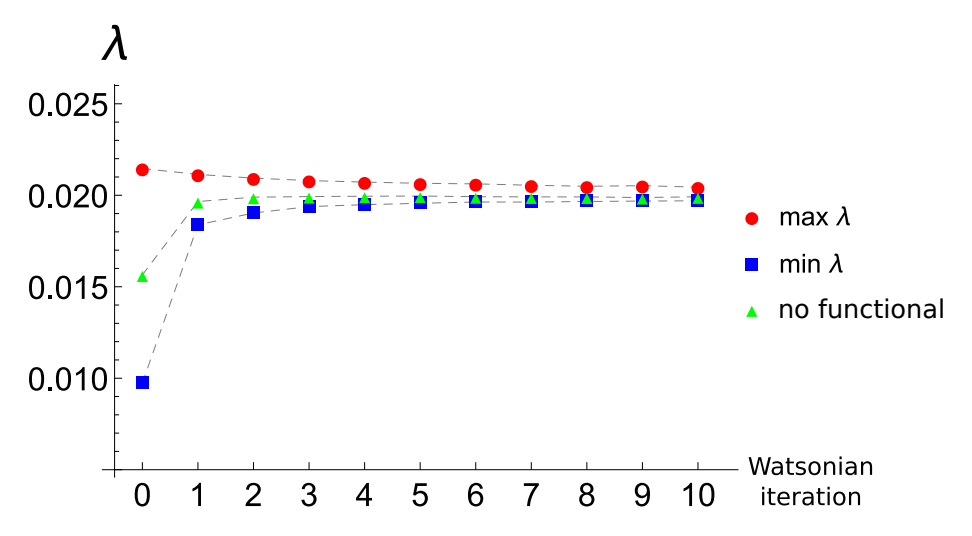


Figure 1: Convergence of max-min λ with Watsonian iterations. maximizing: \bullet , minimizing: \blacksquare , no functional: \blacktriangle

3.2 Test by computing scattering lengths

Here we repeat the calculation of the previous section for the S0, P1, S2 scattering lengths $a_0^{(0)}, a_1^{(1)}, a_0^{(2)}$ defined from:

$$\operatorname{Re} h_{\ell}^{I}(s) \stackrel{k \to 0}{\simeq} \frac{4m_{\pi}}{\sqrt{s}} k^{2\ell+1} \left(a_{\ell}^{I} + b_{\ell}^{I} k^{2} + \dots \right), \quad k = \frac{\sqrt{s - 4m_{\pi}^{2}}}{2} . \tag{3.13}$$

where $S_{\ell}^{I} = 1 + ih_{\ell}^{I}$ as in (2.4). It should be noted that according to the pure S-matrix bootstrap [21], the scattering lengths do not have upper bounds. This seems to be reflected here in the fact that the UV and IR constraints still allow an upper value quite larger than the minimum one. In spite of that, the iteration procedure converges again whether we start from maximum, minimum or just a feasible point. The results are shown in figure 3

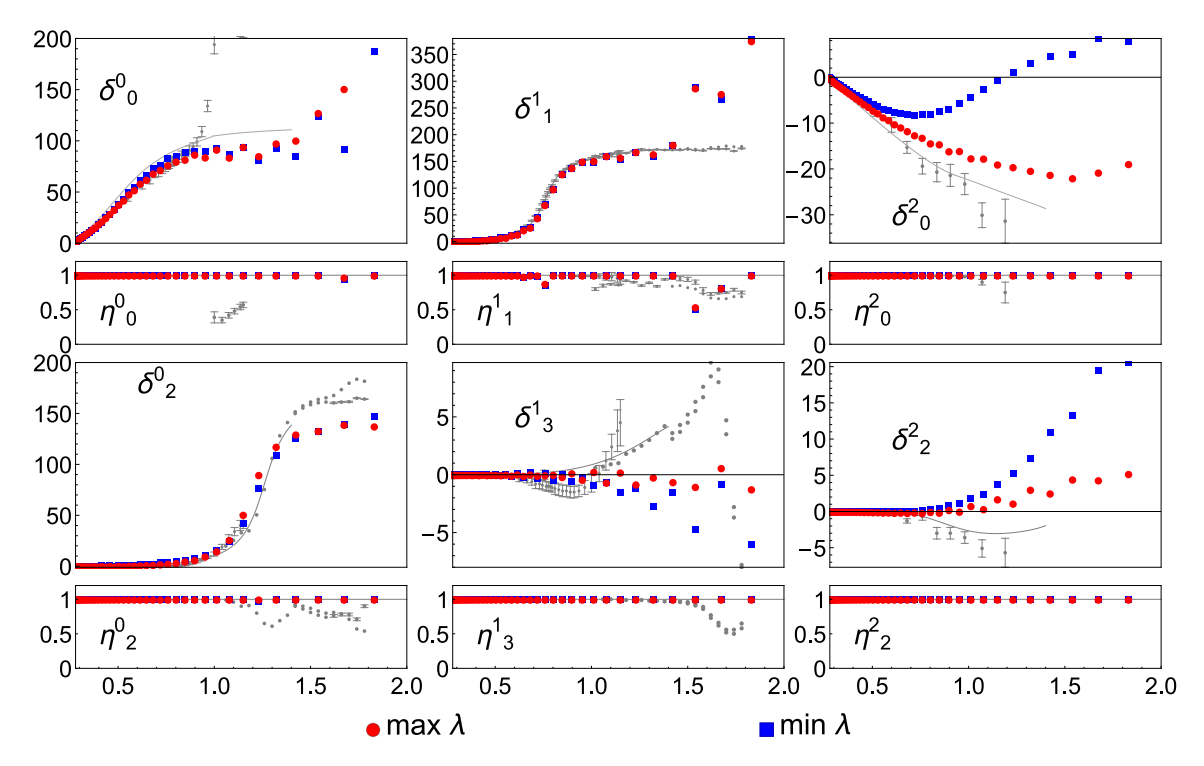


Figure 2: Partial waves of the maximum and minimum λ after 1 Watsonian iteration. As a reference we plot the experimental data from [52–54] (gray dots) as well as phenomenological fits from [5] (gray lines). In the experimental data, the S0 wave has a bump from Kaon pair production that we do not have since we do not include the s quark. Resonances are clearly visible in the S0, P1 and D0 channels.

3.3 Test by computing pion radii

In this case, we show in figure 4 convergence of the iterations for the pion radii defined from an expansion of the form factor around s = 0:

$$F_{\ell}^{I}(s) = F_{\ell}^{I}(0) \left(1 + \frac{1}{6} \langle r_{\pi}^{2} \rangle_{\ell}^{I} + \dots \right)$$
 (3.14)

In summary, these tests show that the procedure uniquely converges to a solution that satisfies all constraints.

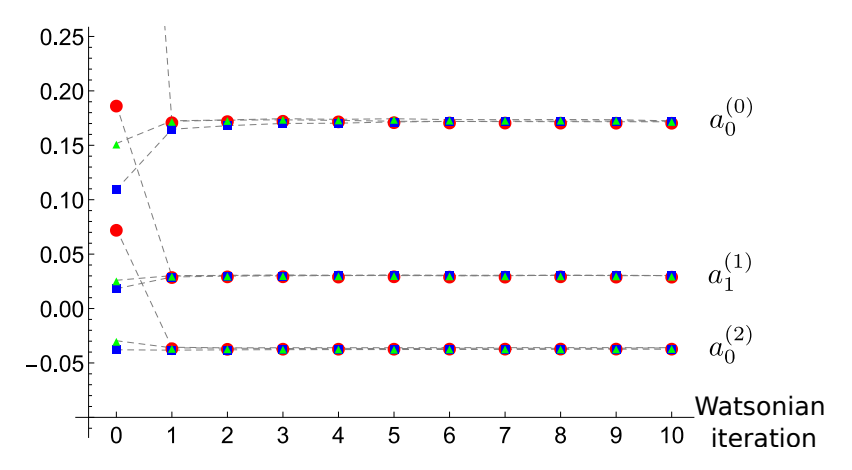


Figure 3: Convergence of max-min $a_{\ell}^{(I)}$ with Watsonian iterations. maximizing: \bullet , minimizing: \blacksquare , no functional: \blacktriangle

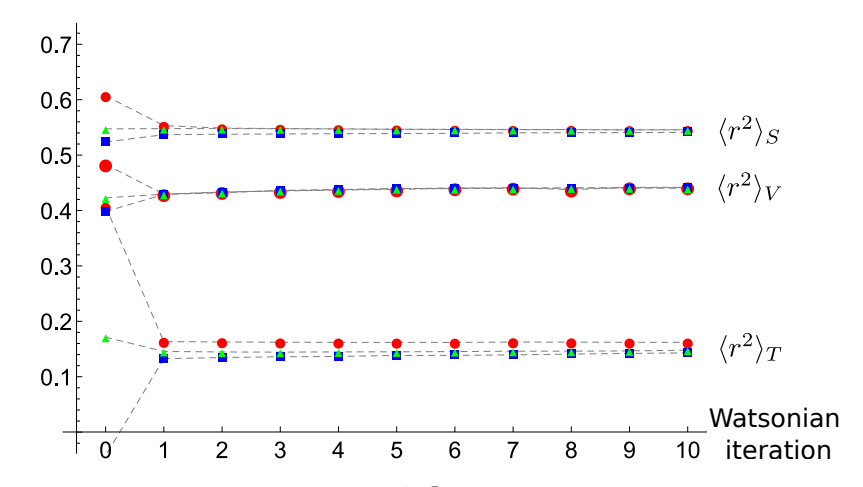


Figure 4: Convergence of max-min $\langle r_\pi^2 \rangle_\ell^I$ with Watsonian iterations. maximizing: \bullet , minimizing: \bullet , no functional: \blacktriangle . As conventional we denote $\langle r_\pi^2 \rangle_0^0 = \langle r_\pi^2 \rangle_S$, $\langle r_\pi^2 \rangle_1^1 = \langle r_\pi^2 \rangle_V$, $\langle r_\pi^2 \rangle_2^0 = \langle r_\pi^2 \rangle_T$, the scalar vector and tensor radii.

4 Detailed study of a converged solution

Having shown that, given some fixed UV data, the procedure converges to a unique solution, we analyze here the properties of the converged solution computing low energy coefficients, scattering lengths, charge radii, etc. In figure 5, we show the partial waves and form factors of the converged solution we obtained in the previous section using no functional, as well as comparison with experimental and phenomenologi-

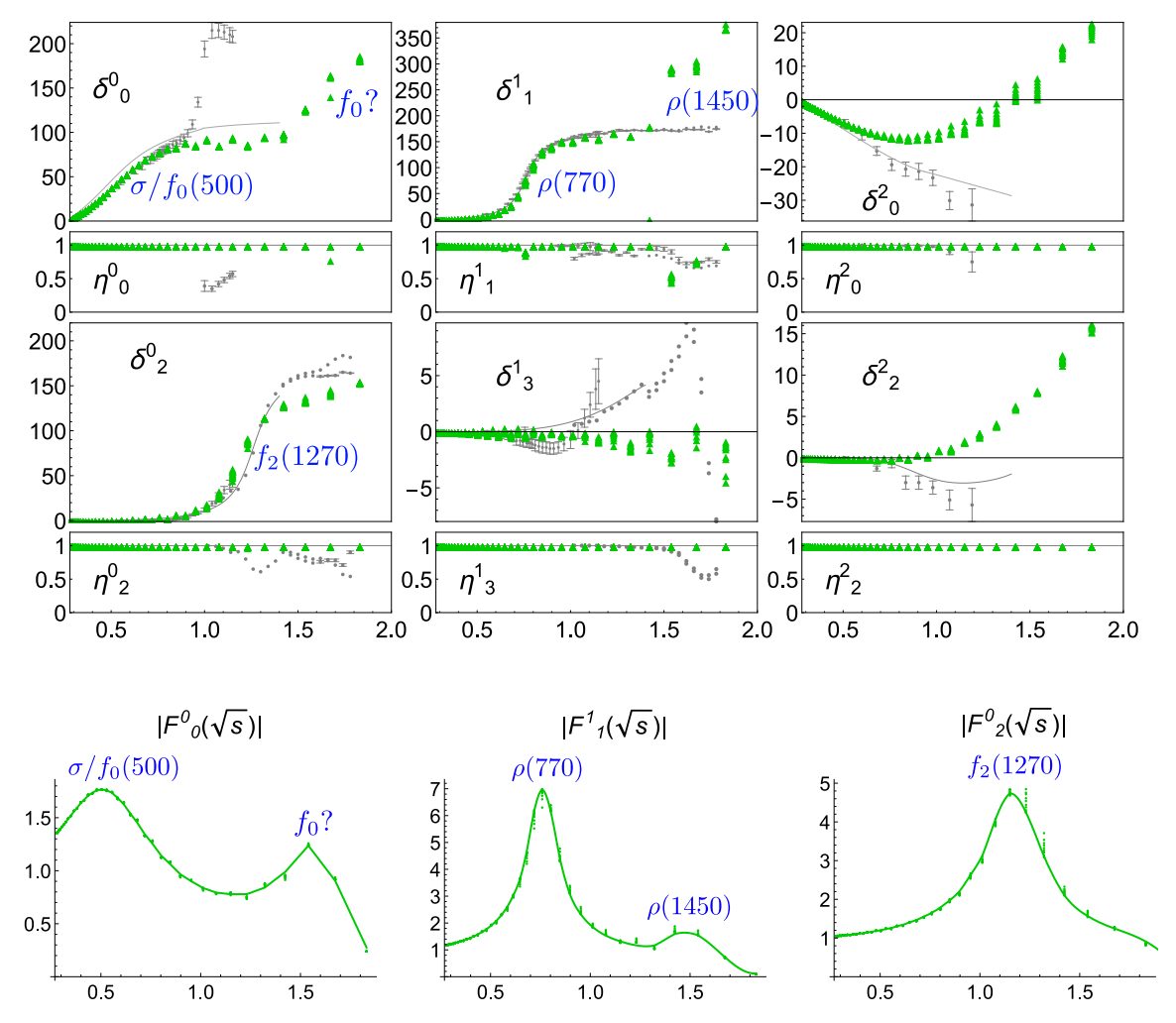


Figure 5: Partial waves and form factors for 10 iterated solutions (\triangle) using nofunctional, namely starting for an arbitrarily feasible point. Horizontal axes are energy/momentum transfer in GeV. The experimental/phenomenological values in gray are the same as in fig. 2.

cal work. In obtaining this, we still keep the values that determine the form factor asymptotics as $\chi_0^0 = 8$, $\chi_1^1 = 2.2$, $\chi_2^0 = 9$ as in (2.10). In section 5 we will study how the results change with those values.

4.1 Low energy parameters and one-loop χ_{PT} amplitude

By comparing the pion scattering amplitude A(s,t,u) of the converged solution with the χ_{PT} one-loop amplitude (see appendix A), we can extract the low energy constants $\bar{\ell}_j$ and the pion coupling λ , and from there the low energy f_{π} using (A.13). Also, we can match the partial waves in fig. 5 with the low energy expansion of the partial waves and form factors in (2.4) and (3.14) (or use dispersion relations) to extract the scattering lengths, effective ranges and pion radii. The results are presented in tables 1,2.

	GTB	GL	Bij	CGL
$ar{\ell}_1$	1.6	-2.3 ± 3.7	$\text{-}1.7 \pm 1.0$	-0.4 ± 0.6
$ar{\ell}_2$	5.5	6.0 ± 1.3	6.1 ± 0.5	4.3 ± 0.1
$egin{array}{c} ar{\ell}_2 \ ar{\ell}_3 \ ar{\ell}_4 \end{array}$	7.8	2.9 ± 2.4		
$ar{\ell}_4$	4.7	4.3 ± 0.9	4.4 ± 0.3	4.4 ± 0.2
$ar{\ell}_6$	14.3	18.7 ± 1.1	$16.0 \pm 0.5 \pm 0.7$	
		Exp.	W	
λ	0.02		0.023	
$f_{\pi} \; (\mathrm{MeV})$	101	92		

Table 1: Comparison of low-energy constants $\bar{\ell}_i$ (see appendix A for definition) computed in this paper (**GTB**) with analysis of experimental results: **GL** [55], **Bij** [6–8], **CGL** [4]. The value of $\lambda = 0.023$ is from the (tree-level) Weinberg model (**W**) (3.12) and $f_{\pi} \simeq 92$ MeV is the standard value [56]. There is reasonable agreement except for $\bar{\ell}_{1,3}$ that are quite difficult to determine.

We can then plot the computed amplitude A(s,t,u) and compare it with the χ_{PT} results using the low energy coefficients we extracted. To simplify the plot we follow the value of the amplitude along a path in the Mandelstam triangle as depicted in fig. 6. The matching is a check of the accuracy of the results.

	GTB	GL	PY	W
$a_0^{(0)}$	0.172	0.220 ± 0.005	0.230 ± 0.010	0.16
$a_0^{(2)}$	-0.0366	-0.0444 ± 0.0010	-0.0422 ± 0.0022	-0.046
$b_0^{(0)}$	0.251	0.280 ± 0.001	0.268 ± 0.010	0.18
$b_0^{(2)}$	-0.063	-0.080 ± 0.001	-0.071 ± 0.004	-0.092
$10^3 \times a_1^{(1)}$	32.1	37.0 ± 0.13	38.1 ± 1.4	31
$10^3 \times b_1^{(1)}$	2.69	5.67 ± 0.13	4.75 ± 0.16	0
$10^4 \times a_2^{(0)}$	12.9	17.5 ± 0.3	18.0 ± 0.2	0
$10^4 \times a_2^{(2)}$	-1.1	1.70 ± 0.13	2.2 ± 0.2	0
		Exp. fits		
$\langle r^2 \rangle_S^{\pi} (\text{fm}^2)$	0.55	0.61 ± 0.04		
$\langle r^2 \rangle_V^{\pi} \; (\mathrm{fm}^2)$	0.441	0.439 ± 0.0087		
$\langle r^2 \rangle_T^{\pi} (\text{fm}^2)$	0.146			

Table 2: Comparison of scattering lengths and pion radii as computed here (**GTB**) with experimental values from **GL** [55], **PY** [5] and the tree level Weinberg model (**W**) [57].

4.2 Resonances

As seen in fig. 5, the partial waves and form factors display very clear resonances in the P1 and D0 channel whose width and masses can be extracted by fitting the form factors with a Breit-Wigner shape. The results are summarized in table 3. Once again we would like to emphasize that no assumption was made on the number of resonances or any other property of the spectrum. The existence of these resonances is a result of the calculation. Finally, one can notice broad resonances in the S0 channel, the well-known $\sigma/f_0(500)$ whose nature is somewhat controversial [58] (and perhaps additional f_0 states) that we do not list in the table. Also, the P1 form factor is of interest due to its relation to the hadronic ratio R [56] that measures hadronic photo-production in e^+e^- collisions. We compare the results of this paper with experiment in fig. 7. The agreement is good although we are basically showing

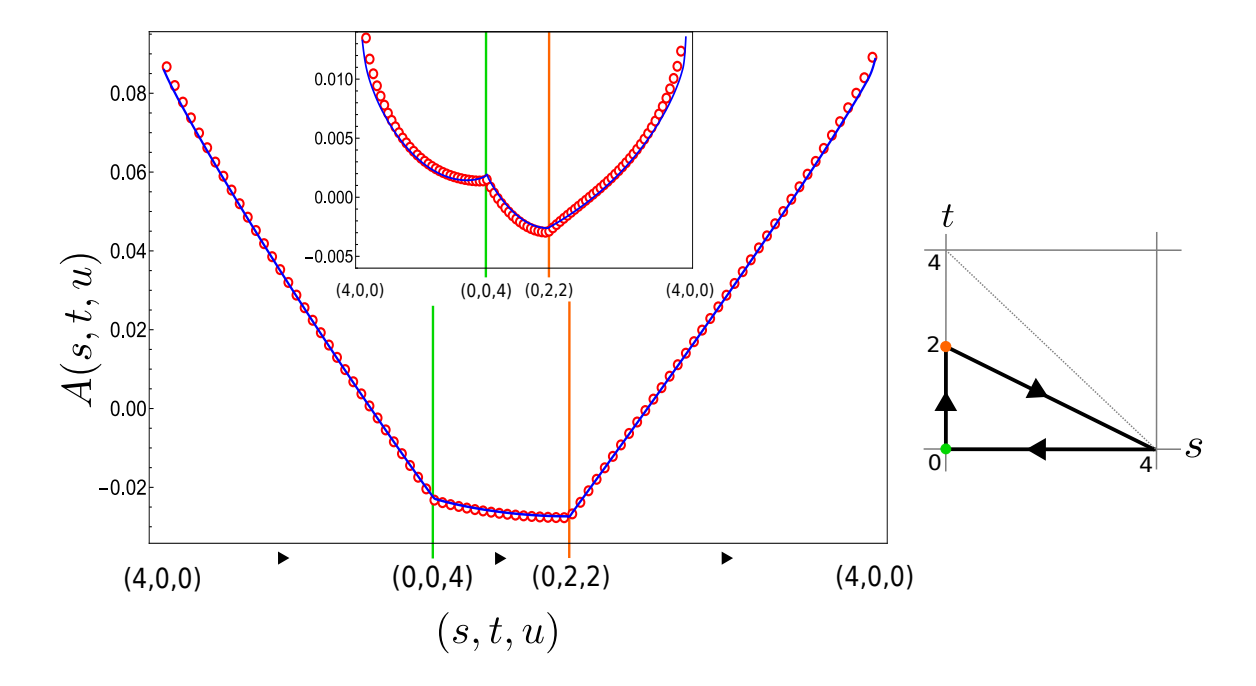


Figure 6: We follow the value of the pion scattering amplitude A(s,t,u) = A(s,u,t) along the path indicated on the right in the (s,t) plane. The blue line is the prediction of χ_{PT} using tree-level plus one-loop with the values of the constants extracted from our result as shown in table 1. The red circles are the results of the GTB converged solution. The inset depicts the same with the tree-level part removed.

the ρ meson dominance of the form factor.

5 Dependence on the input parameters

5.1 Form factor asymptotics

As mentioned before, an input of the procedure is the asymptotic value of the form factors. In the literature it has been argued, for example, that, at 2GeV the P1 form factor can differ from the Brodsky-Lepage value [35,59] by a factor up to 3 [46]. For that reason we explore how the ρ mass and width, the f_2 mass and width change as a function of this parameter starting from minimal feasible value. The results are in figures 8, 9, 10, 11.

	GTB	PDG	
$m_{ ho}$	758	775 ± 0.23	MeV
$\Gamma_{ ho}$	137	149.1 ± 0.8	${ m MeV}$
$m_{ ho'}$	1514	1465 ± 25	${ m MeV}$
$\Gamma_{ ho'}$	162	400 ± 60	${ m MeV}$
m_{f_2}	1180	1275.4 ± 0.8	${ m MeV}$
Γ_{f_2}	249	186.6 ± 2.3	MeV

Table 3: Masses and widths of the most prominent resonances. The results are similar and compatible with our previous work [1,2] and agree reasonably well with the known experimental results [56].

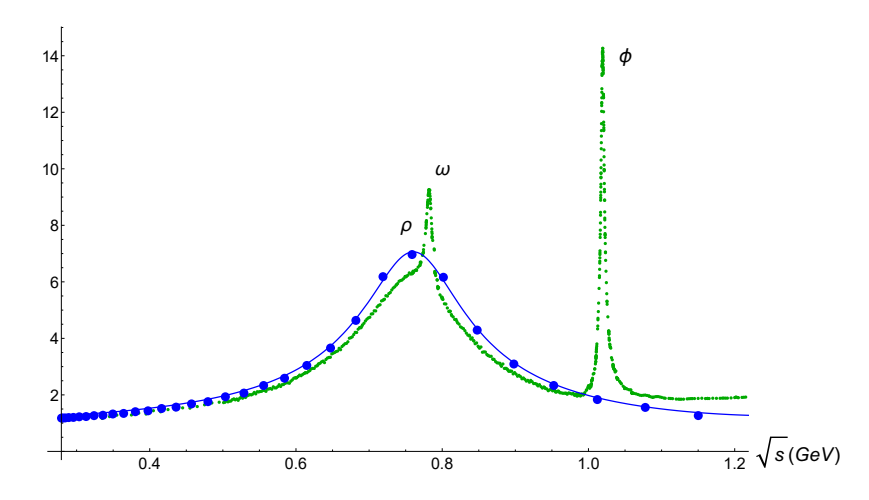


Figure 7: In green hadronic R-ratio taken from [56] and rescaled to match the vector form factor $|F_1^1|$ and compared with the present result (blue). The $N_f=2$ vector current does not couple to the ω and ϕ resonances so we do not see those peaks. The agreement is reasonable and of interest in computations of the hadronic contributions to g-2 based on this method [34]

5.2 Low energy tolerance

For completeness we also study the dependence of the converged solution on the tolerance used to match the low energy partial waves [1,2]. At low energy we choose a small set of points s_j in the very low energy unphysical region $0 < s_j \le 2$, and

require that

$$||f_0^0(s_j) - R_{01}^{\text{tree}}(s_j)f_1^1(s_j)|| \le \epsilon^{\chi},$$

$$||f_0^2(s_j) - R_{21}^{\text{tree}}(s_j)f_1^1(s_j)|| \le \epsilon^{\chi},$$

$$R_{01}^{\text{tree}} = \frac{f_{0,\text{tree}}^0}{f_{1,\text{tree}}^1}, \quad R_{21}^{\text{tree}} = \frac{f_{0,\text{tree}}^2}{f_{1,\text{tree}}^1}$$
(5.15)

with some tolerance e^{χ} . The values referred as "tree" are from the tree level Weinberg model (A.2). The results for various values of the tolerance e^{χ} are displayed in fig.12. Once again, the Watsonian iteration removes the dependence on this parameter except somewhat for the I=2 channels (and also spin 3) where we do not have UV input.

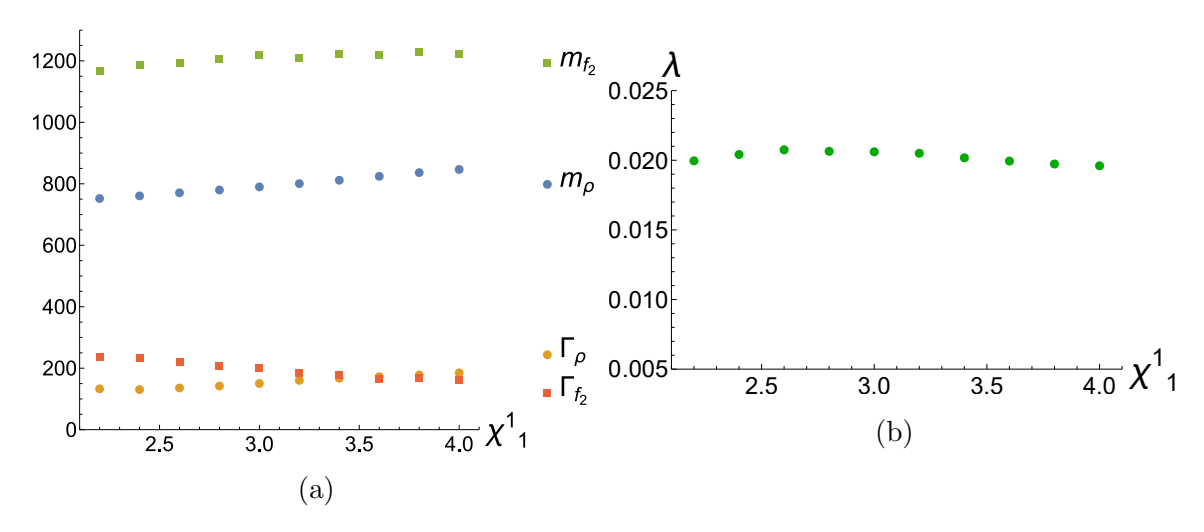


Figure 8: the ρ , f_2 meson mass and width (in MeV) (8a) and pion coupling λ (8b) for form factor asymptotic factor $2.2 \le \chi_1^1 \le 4$.

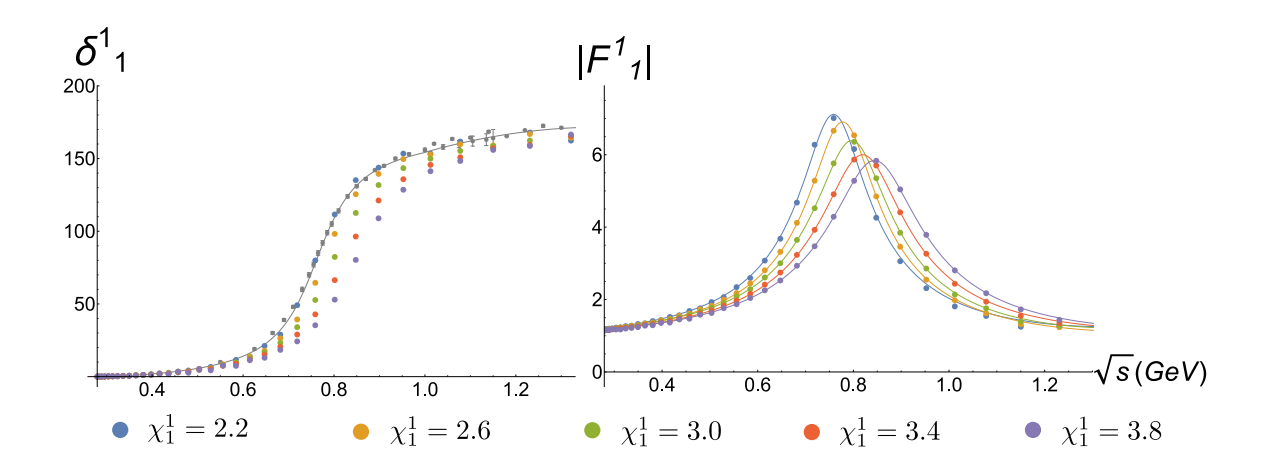


Figure 9: The P1 phase shift δ_1^1 and vector form factor $|F_1^1(s)|$ for form factor asymptotic factor $2.2 \le \chi_1^1 \le 3.8$

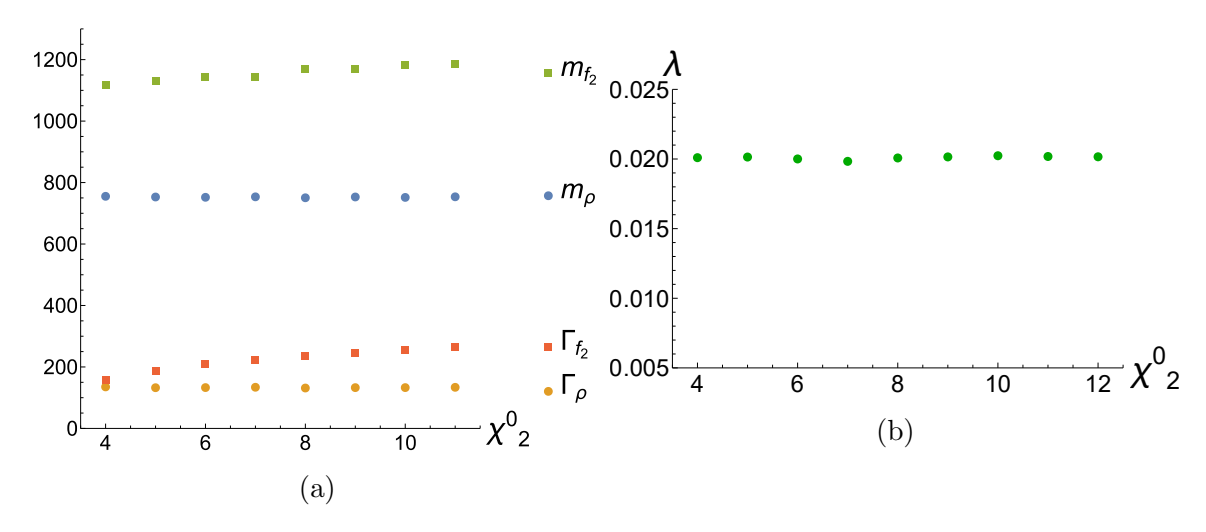


Figure 10: the ρ , f_2 meson mass and width (in MeV) (10a) and pion coupling λ (10b) for form factor asymptotic factor $4 \le \chi_2^0 \le 12$.

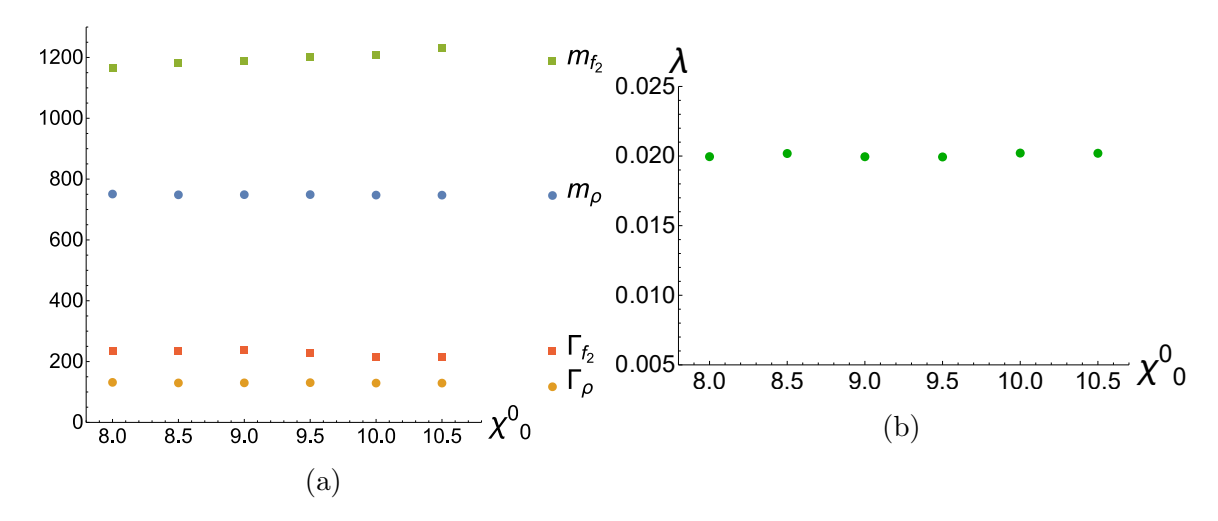


Figure 11: the ρ , f_2 meson mass and width (in MeV) (11a) and pion coupling λ (11b) for form factor asymptotic factor $8 \le \chi_0^0 \le 10.5$.

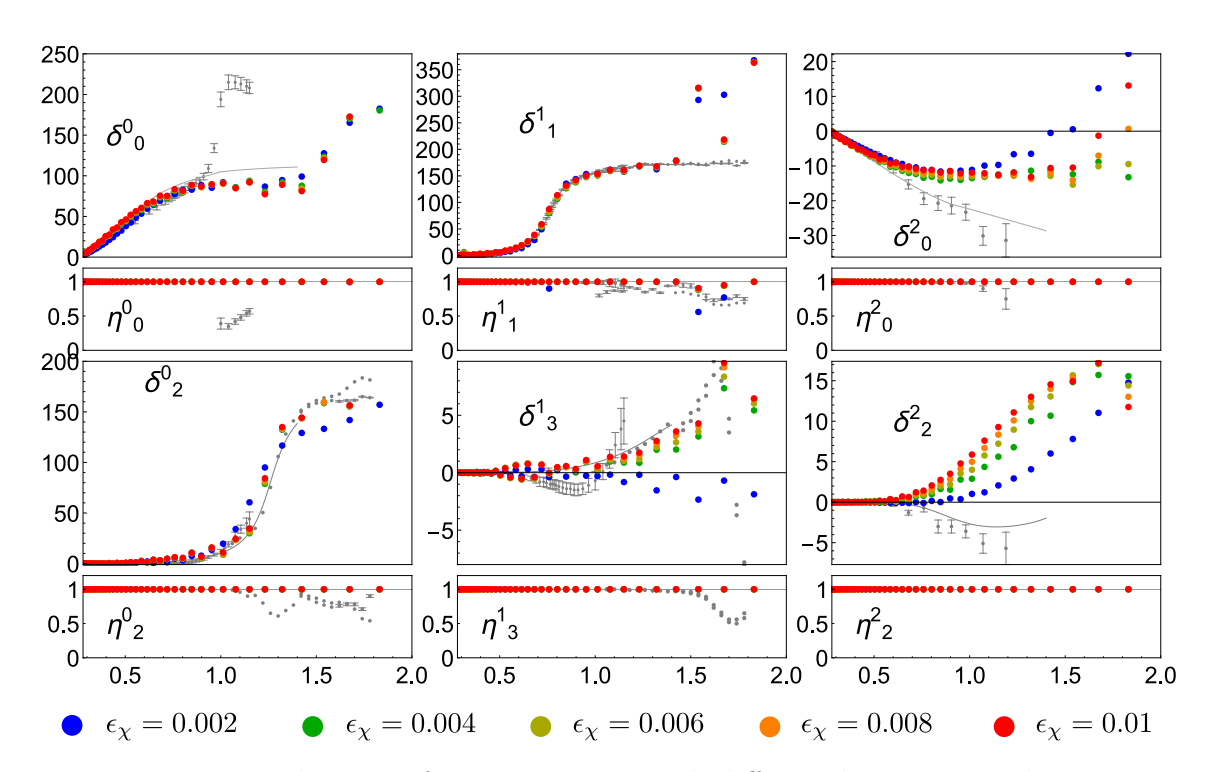


Figure 12: Partial waves after 10 iteration with different low energy tolerance ϵ_{χ}

6 Thermodynamics of a dilute gas of pions, second virial coefficients and density of pion pairs

The computation of the two particle elastic S-matrix allows us to study the thermodynamics properties of a pion gas in the low density and low energy region [60, 61]. A dilute gas of bosons is such that each single particle state ϵ_{α} has a low occupation number $n_{\alpha} \ll 1$. In that case, the virial expansion determines the partition function in terms of the single particle partition function with corrections from two particle elastic scattering that we can compute from our results in a similar way as done in [62] based on experimental phase shifts. This is part of a more general program of computing the thermodynamics of relativistic gases based on the scattering matrix [61]. See also [63] for a recent discussion in the context of QCD strings. Briefly, the grand canonical partition function Ξ can be expanded in powers of the fugacity $z = e^{\beta \mu}$ as

$$\beta P = \lim_{V \to \infty} \frac{1}{V} \ln \Xi = \sum_{n=1}^{\infty} b_n(T) z^n$$
 (6.16)

where e.g. from [62] we have

$$b_1 = 3 \int \frac{d^3p}{(2\pi\hbar)^3} e^{-\beta\sqrt{p^2 + m_\pi^2}} = \frac{3m_\pi^2}{2\pi^2\hbar^3\beta} K_2(\beta m_\pi)$$
 (6.17a)

$$b_2 = \frac{1}{2\pi^3 \beta} \int_{2m_{\pi}}^{\infty} dM \, M^2 K_2(\beta M) \sum_{I\ell} (2I+1)(2\ell+1) \frac{\partial \delta_{\ell}^I}{\partial M}$$
 (6.17b)

where $K_2(x)$ is a standard modified Bessel function and δ_ℓ^I are the scattering phaseshifts. If pions are created by a transition from an unconfined phase, the number of pions will maximize the entropy and therefore the chemical potential would be zero. In general one would also expect $\mu = 0$ since the number of pions is not conserved, but inelastic scattering is highly suppressed in the dilute gas and low energy approximations so an effective μ can appear. Presumably we can even have Bose-Einstein condensation. However this is only on the assumption that electromagnetic and weak interactions are disconnected so that pions are stable (as in lattice calculations for example).

From here we can compute the pressure as a function of temperature (for $\mu = 0$)

$$P_{\text{int}} = Tb_2, \ \epsilon_{\text{int}} = -\frac{\partial b_2}{\partial \beta}, \ n_{\text{int}} = 2b_2, \ s_{\text{int}} = \left[b_2 \left(1 - 2\mu\beta\right) - \beta \frac{\partial b_2}{\partial \beta}\right]$$
 (6.18)

where "int" denotes the interaction correction to the ideal gas expressions. The results are displayed in fig.13 and, as expected are similar to those in [62].

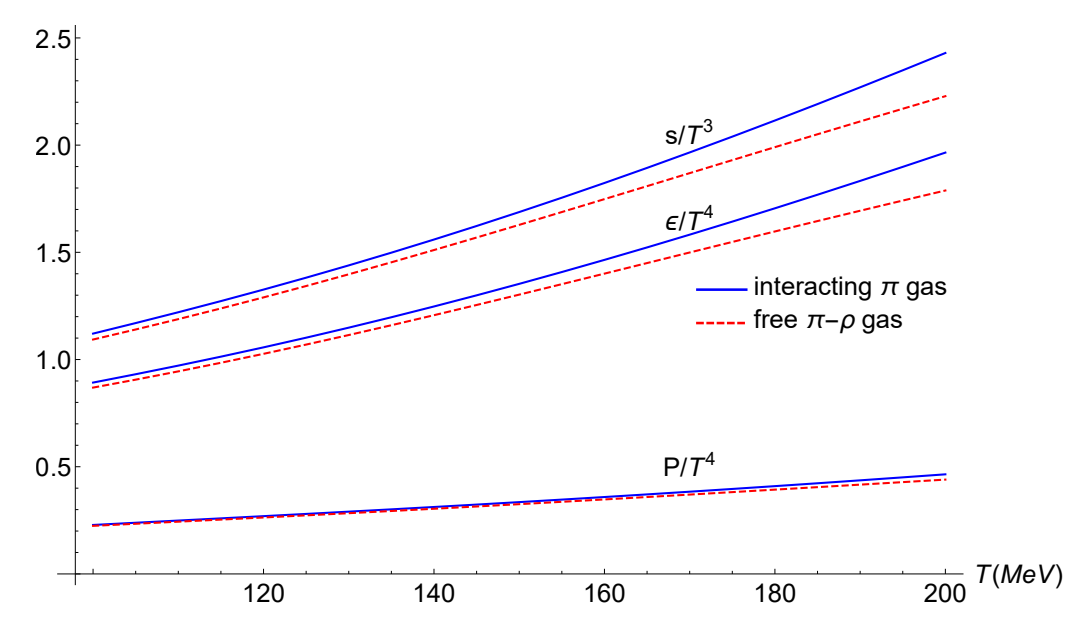


Figure 13: Thermodynamic quantities (pressure P, energy density ϵ , entropy density s) of a dilute interacting pion gas as a function of temperature for $\mu = 0$, computed from the phase shifts we obtained (fig. 5). We compare with a free gas of pions and ρ mesons. As discussed in [62] the results are similar.

A quantity that is of interest for pions produced in high energy nuclear collisions⁷ [64], when the quark gluon plasma cools down, is the difference in the pairs of pions with opposite (electric) charge $N_{\rm OS}$ minus the number of pairs with the same sign $N_{\rm SS}$. For free pions this difference vanishes if we compute it as $N_{\rm OS} - N_{\rm SS} = 2\langle\langle n_+\rangle\rangle\langle\langle n_-\rangle\rangle - \langle\langle n_+\rangle\rangle\langle\langle n_+\rangle\rangle - \langle\langle n_-\rangle\rangle\langle\langle n_-\rangle\rangle$ since $\langle\langle n_+\rangle\rangle = \langle\langle n_-\rangle\rangle$ The interactions produce a difference in the number of pairs giving, at the lowest order of the virial expansion:

$$N_{\text{OS}} - N_{\text{SS}} = V z^2 \int_{2m_{\pi}}^{\infty} n_{os-ss}(M) dM$$

$$n_{os-ss}(M) = \frac{M^2}{2\pi^2 \beta} K_2(\beta M) \sum_{\ell} \frac{2\ell+1}{\pi} \frac{\partial}{\partial M} \left\{ \frac{1}{3} \delta_{\ell}^{I=0} - \frac{5}{6} \delta_{\ell}^{I=2} + \frac{1}{2} \delta_{\ell}^{I=1} \right\}$$
(6.19)

where the \sum' indicates that we only sum (for each term) the angular momentum allowed for that isospin (even for I = 0, 2 and odd for I = 1). Also, M is the

⁷We are grateful to Fuqiang Wang for a discussion on this topic.

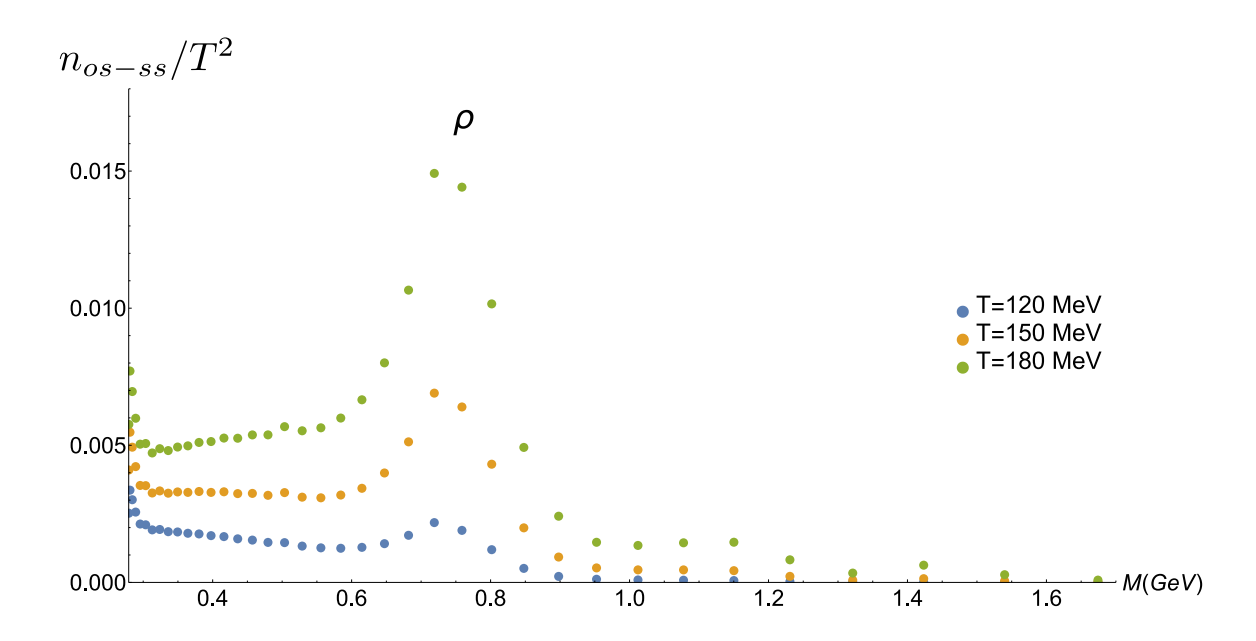


Figure 14: From (6.19), n_{os-ss}/T^2 , *i.e.* density of pairs of pions with opposite sign minus same sign distributed over the invariant mass M and normalized with T^2 . The results are for a dilute gas of pions using the phase shifts obtained in this paper. The chemical potential is taken to be $\mu = 0$.

invariant mass of the pair $(M^2 = (p_1 + p_2)^2)$, and, for the case of zero chemical potential $(\mu = 0)$, we have z = 1. The results are depicted in fig. 14. The ρ resonance peak coming from $\frac{\partial \delta_1^1}{\partial M}$ is evident. It can be interpreted as an increase in the density of states near the ρ mass or as ρ mesons being created and destroyed leading in both cases to an extra density of pairs of opposite sign.

7 Conclusions

The goal of the Gauge Theory Bootstrap is to completely determine the dynamics of asymptotically free gauge theories (QCD) in the strongly coupled regime where perturbative QCD does not apply and neither does the low energy effective pion Lagrangian. An important point is that the only stable particles are pions (assuming no other interactions are present and ignoring nucleons) and therefore pions are the only asymptotic states in that energy region. The idea is then to constrain the dynamics using input from the very low energy Lagrangian (using m_{π}) and from high energy using sum rules and asymptotic form factors. Notice that the

leading asymptotic form factors are basically controlled by the pion radius that is determined by f_{π} . Therefore we also need, from low energy at least the order of magnitude of f_{π} . Given those and the gauge theory parameters we expect to find a unique pion scattering matrix, form factors, spectral densities, etc. In this paper we introduce an iterative procedure that, given the UV and IR information, converges to a unique answer which we take to be the result of the computation. By maximizing and minimizing various physical quantities (like couplings, scattering lengths, etc.) we show that there is a small space of qualitatively similar solutions around the converged one providing an estimate on the error of the computation. Another source of error is the fact that the asymptotic values of the form factors are not predicted from QCD very precisely. Finally there is a systematic error due to the fact that we take the converged solution as the best estimate of the physical solution. This could be improved, for example, by including more operators in each channel. We expect to explore this more in future work.

8 Acknowledgements

We are grateful to Lance Dixon, Nick Manton, Ian Moult, Massimiliano Procura and Arkady Vainshtein for many interesting discussions on the topics of this paper. Y.H. is grateful to CERN for hospitality while this work was being completed. This work was supported in part by DOE through the QuantiSED Fermilab consortium.

A Chiral Lagrangian and one-loop amplitude

The very low energy description of pion dynamics is given by the non-linear sigma model:

$$\mathcal{L}_2 = \frac{F^2}{4} \text{Tr}[D_\mu U D^\mu U^\dagger] + \frac{F^2}{4} \text{Tr}(\chi U^\dagger + U \chi^\dagger)$$
 (A.1)

where $U = \exp(i\pi^a \tau_a/F)$ and covariant derivatives include external gauge fields as sources. Also χ is a source whose expectation value determines the pion mass⁸. We refer to [40,55] for the notation and main summary of the chiral perturbation theory approach. In particular, in this appendix we follow [55] and denote as F, M the parameters of the effective action whereas f_{π} , m_{π} denote the physical values of the pion decay constant and mass (see (A.5) below). At this order, the pion scattering

⁸It is conventional to call this source χ as we do in this appendix. It should not be confused with χ_{ℓ}^{I} in the main text that represents the factors in the form factor asymptotics.

amplitude is

$$A_{\text{tree}}(s, t, u) = \frac{s - M^2}{8\pi^2 F^2} \tag{A.2}$$

This is the $t \leftrightarrow u$ symmetric part. The full amplitude for $\pi_a(p_1) + \pi_b(p_2) \to \pi_c(p_3) + \pi_d(p_4)$ is written as

$$T_{ab,cd} = A(s,t,u)\delta_{ab}\delta_{cd} + A(t,s,u)\delta_{ac}\delta_{bd} + A(u,t,s)\delta_{ad}\delta_{bc}$$
(A.3)

where a, b, c, d are isospin one indices. The higher energy corrections were studied systematically by Gasser and Leutwyler in the same work [40] leading to the definition of a number of low energy (or Wilson) coefficients $\bar{\ell}_j$ through the Lagrangian [40]:

$$\mathcal{L}_{4} = \frac{l_{1}}{4} \left\{ \text{Tr}[D_{\mu}U(D^{\mu}U)^{\dagger}] \right\}^{2} + \frac{l_{2}}{4} \text{Tr}[D_{\mu}U(D_{\nu}U)^{\dagger}] \text{Tr}[D^{\mu}U(D^{\nu}U)^{\dagger}]
+ \frac{l_{3}}{16} [\text{Tr}(\chi U^{\dagger} + U\chi^{\dagger})]^{2} + \frac{l_{4}}{4} \text{Tr}[D_{\mu}U(D^{\mu}\chi)^{\dagger} + D_{\mu}\chi(D^{\mu}U)^{\dagger}]
+ l_{5} \left[\text{Tr}(f_{\mu\nu}^{R}Uf_{L}^{\mu\nu}U^{\dagger}) - \frac{1}{2} \text{Tr}(f_{\mu\nu}^{L}f_{L}^{\mu\nu} + f_{\mu\nu}^{R}f_{R}^{\mu\nu}) \right]
+ i \frac{l_{6}}{2} \text{Tr}[f_{\mu\nu}^{R}D^{\mu}U(D^{\nu}U)^{\dagger} + f_{\mu\nu}^{L}(D^{\mu}U)^{\dagger}D^{\nu}U]
- \frac{l_{7}}{16} [\text{Tr}(\chi U^{\dagger} - U\chi^{\dagger})]^{2}$$
(A.4)

At one loop one introduces the renormalized constants $\bar{\ell}_j$ defined at a renormalization scale $\mu = m_{\pi}$ [55]. It also gives the physical m_{π} , f_{π} as [55]

$$m_{\pi}^{2} = M^{2} \left\{ 1 - \frac{M^{2}}{32\pi^{2}F^{2}}\bar{\ell}_{3} + \mathcal{O}(M^{4}) \right\}$$
 (A.5)

$$f_{\pi} = F \left\{ 1 + \frac{M^2}{16\pi^2 F^2} \bar{\ell}_4 + \mathcal{O}(M^4) \right\}$$
 (A.6)

Although all this is well known, we include it here to give the definition of $\bar{\ell}_j$ and as a reference point for interpreting our results in comparison with other work. Notice, however, that our main focus is the intermediate energy region where pions are strongly coupled, namely where this Lagrangian does not apply. In chiral perturbation theory the low energy constants $\bar{\ell}_i$ are determined from fitting with experiments but in the Gauge Theory Bootstrap approach they are computed from QCD (under certain assumptions).

One way to compute the $\bar{\ell}_j$'s is to match the amplitude we obtain in GTB to the tree-level plus one-loop result from [55] (replacing M by m_{π} using (A.5)):

$$A(s,t,u) = \frac{s - m_{\pi}^2}{8\pi^2 F^2} - \frac{\bar{\ell}_3}{256\pi^4 F^4} + \frac{1}{768\pi^4 F^4} (A_1(s,t,u) + A_2(s,t,u)) + \mathcal{O}(p^6) \quad (A.7)$$

where

$$A_1(s,t,u) = 3(s^2 - m_\pi^4)I_f(s) + (t(t-u) - 2tm_\pi^2 + 4um_\pi^2 - 2m_\pi^4)I_f(t)$$

$$+(u(u-t) - 2um_\pi^2 + 4tm_\pi^2 - 2m_\pi^4)I_f(u)$$
(A.8a)

$$A_2(s,t,u) = 2\left(\bar{\ell}_1 - \frac{4}{3}\right)(s - 2m_\pi^2)^2 + \left(\bar{\ell}_2 - \frac{5}{6}\right)(s^2 + (t-u)^2) - 12sm_\pi^2 + 15m_\pi^4$$

with

$$I_f(s) = \beta(s) \ln\left(\frac{\beta(s) - 1}{\beta(s) + 1}\right) + 2, \quad \beta(s) = \sqrt{1 - \frac{4m_\pi^2}{s}}$$
 (A.9)

For $0 < s < 4m_{\pi}^2$ the expression

$$I_f(s) = 2 - 2\sqrt{\frac{4m_\pi^2}{s} - 1} \operatorname{arccot}\left(\sqrt{\frac{4m_\pi^2}{s} - 1}\right)$$
 (A.10)

is also useful. Introducing λ as defined in (3.11), we obtain (we now set $m_{\pi} = 1$ as in most of the paper):

$$\lambda = \frac{1}{32\pi F^2} \left(1 + \frac{1}{96F^2} (1 - \sqrt{2}\arctan(2\sqrt{2})) + \frac{1}{39F^2} (\bar{\ell}_1 + \bar{\ell}_2) \right) + \mathcal{O}\left(\frac{1}{F^6}\right)$$
(A.11)

We also get:

$$A(s,t,u) = \frac{4}{\pi}\lambda(s-1) + \frac{4\lambda^2}{3\pi^2} \left[A_1(s,t,u) + A_2(s,t,u) - 3(s-1)(\bar{A}_1 + \bar{A}_2 - 3\bar{\ell}_3) - 3\bar{\ell}_3 \right]$$

where $\bar{A}_{1,2} = A_{1,2}(\frac{4}{3}, \frac{4}{3}, \frac{4}{3})$. In particular notice the dependence on the coefficients $\bar{\ell}_{1,2,3}$:

$$A(s,t,u;\bar{\ell}_1,\bar{\ell}_2,\bar{\ell}_3) = A(s,t,u;0,0,0) + \frac{4\lambda^2}{3\pi^2} \left[2\bar{\ell}_1(s-2)^2 + \bar{\ell}_2(s^2 + (t-u)^2) - \frac{8}{3}(s-1)(\bar{\ell}_1 + 2\bar{\ell}_2 - \frac{27}{8}\bar{\ell}_3) - 3\bar{\ell}_3 \right]$$
(A.12)

The physical value of f_{π} is related to λ through

$$\frac{1}{f_{\pi}^{2}} = 32\pi\lambda - \frac{32}{9}\lambda^{2} \left(8\bar{l}_{1} + 16\bar{l}_{2} - 27\bar{l}_{3} + 36\bar{l}_{4} + 33 - 33\sqrt{2}\tan^{-1}\left(2\sqrt{2}\right)\right) + \mathcal{O}(\lambda^{3})$$
(A.13)

It is interesting to study the amplitude in the Mandelstam triangle defined by s > 0, t > 0, u > 0. Since A(s,t,u) is symmetric under the interchange $t \leftrightarrow u$, we only need the subregion t < u. To simplify the plots we just consider the amplitude along the boundary of that triangle, as depicted in figure 6. By matching the results of the computation with (A.12) we determine the values of $\bar{\ell}_{1,2,3}$. Further we can write the form factors near s = 0 and at lowest non-trivial order as:

$$F_0^{(0)}(s) = 1 + \frac{2\lambda}{\pi} s \left(\bar{\ell}_4 - \frac{13}{12}\right) + \mathcal{O}(\lambda^2)$$
 (A.14a)

$$F_1^{(1)}(s) = 1 + \frac{\lambda}{3\pi} s \left(\bar{\ell}_6 - 1\right) + \mathcal{O}(\lambda^2)$$
 (A.14b)

and use them to the determine $\bar{\ell}_{4,6}$. These expressions are used in the main text to obtain the results in table 2. As a check and to get an idea of the errors in our computation, we can use the values in table 2 to recompute the scattering lengths from [55]:

$$a_0^{(0)} = 7\lambda + \frac{\lambda^2}{9\pi} \left[64\bar{\ell}_1 + 128\bar{\ell}_2 + 144\bar{\ell}_3 + 84 + 231\sqrt{2}\tan^{-1}(2\sqrt{2}) \right] + \mathcal{O}(\lambda^3)$$

$$a_0^{(2)} = -2\lambda + \frac{2\lambda^2}{9\pi} \left[32\bar{\ell}_1 + 64\bar{\ell}_2 - 36\bar{\ell}_3 + 42 - 33\sqrt{2}\tan^{-1}(2\sqrt{2}) \right] + \mathcal{O}(\lambda^3)$$

$$a_1^{(1)} = \frac{4\lambda}{3} + \frac{2\lambda^2}{27\pi} \left[-64\bar{\ell}_1 + 16\bar{\ell}_2 + 54\bar{\ell}_3 - 131 + 66\sqrt{2}\tan^{-1}(2\sqrt{2}) \right] + \mathcal{O}(\lambda^3)$$

$$a_2^{(0)} = \frac{32\lambda^2}{45\pi} \left[\bar{\ell}_1 + 4\bar{\ell}_2 - \frac{53}{8} \right] + \mathcal{O}(\lambda^3)$$

$$a_2^{(2)} = \frac{32\lambda^2}{45\pi} \left[\bar{\ell}_1 + \bar{\ell}_2 - \frac{103}{40} \right] + \mathcal{O}(\lambda^3)$$
(A.15)

and compare with the values in table 2 extracted directly from the partial waves. See table 4 for the comparison.

B Parameterization of the spectral density

In this appendix we describe the parameterizations used for the spectral density, designed to satisfy the correct low energy behavior as described in section 2.1. Consider, for example the vector current with the behavior (2.2b) at lowest order in

	GTB	GTB 2
$a_0^{(0)}$	0.172	0.170
$a_0^{(2)}$	-0.0366	-0.0363
$10^3 \times a_1^{(1)}$	32.1	29.7
$10^4 \times a_2^{(0)}$	12.9	15.0
$10^4 \times a_2^{(2)}$	-1.1	4

Table 4: The scattering lengths extracted directly from the partial waves (**GTB**) comparing with the ones calculated from our low energy constants $\bar{\ell}_i$ computation using (A.15) (**GTB 2**). They are consistent except the I=2 scattering length that presently seems difficult to compute in this approach.

 χ_{PT} [40] in our conventions. Setting $m_{\pi} = 1$, for $s \in \mathbb{R}_{\geq 4}$:

$$\rho_1^1(s) = \frac{1}{(2\pi)^4} \frac{s}{24\pi} \left(1 - \frac{4}{s} \right)^{\frac{3}{2}} = \frac{1}{(2\pi)^4} \frac{1}{192\pi} (s - 4)^{\frac{3}{2}} \left[1 - \frac{3}{8} (s - 4) + \frac{15}{128} (s - 4)^2 + \dots \right]$$
(B.16)

This suggest parameterizing a general ρ , in the region $4 \le s \le s_0$ as

$$\rho_1^1(s) = \frac{1}{(2\pi)^4} \frac{1}{192\pi} (s-4)^{\frac{3}{2}} \left[B + \sum_{n>0} b_n (s-4)^n \right]$$
 (B.17)

Here B is a variable and so are the b_n . Although the powers $(s-4)^n$ provide a basis in this interval, such functions grow as $s \to \infty$. To avoid this we consider the map we have already been using

$$z = \frac{\sqrt{4 - s_a} - \sqrt{4 - s}}{\sqrt{4 - s_a} + \sqrt{4 - s}}$$
 (B.18)

such that

$$\operatorname{Im}[(1-z)^{2k+1}] = (-1)^k 2^{2k+1} \left(\frac{s-4}{4-s_a}\right)^{k+\frac{1}{2}} (1+\mathcal{O}(s-4))$$
 (B.19)

Based on the previous parameterization we can write a parameterization that respects the leading behavior with functions that remain finite at $s \to \infty$ (or $z \to -1$):

$$\rho_0^0 = -\frac{1}{(2\pi)^4} \frac{3}{64\pi} \left(1 - \frac{s_a}{4} \right)^{\frac{1}{2}} \operatorname{Im} \left\{ (1 - z) \left[A + (1 - z) \sum_{n=0}^{N} a_n z^n \right] \right\}$$
 (B.20)

$$\rho_1^1 = +\frac{1}{(2\pi)^4} \frac{1}{96\pi} \left(1 - \frac{s_a}{4} \right)^{\frac{3}{2}} \operatorname{Im} \left\{ (1-z)^3 \left[B + (1-z) \sum_{n=0}^N b_n z^n \right] \right\}$$
(B.21)

$$\rho_2^0 = -\frac{1}{(2\pi)^4} \frac{1}{640\pi} \left(1 - \frac{s_a}{4} \right)^{\frac{5}{2}} \operatorname{Im} \left\{ (1 - z)^5 \left[C + (1 - z) \sum_{n=0}^{N} c_n z^n \right] \right\} (B.22)$$

The coefficients A,B,C and a_n , b_n and c_n are the parameters. These parameterizations allow even powers of (1-z) adding more flexibility. Finally, to make sure that the leading term dominates, we regulate the coefficients by requiring $|a_n| \leq a_{max}$, $|b_n| \leq b_{max}$, $|c_n| \leq c_{max}$. The value of the regulator should be chosen in a range that does not affect the results.

C Finite energy sum rules up to 3-loop

The SVZ sum rules have played a major role in the understading of hadrons from QCD and therefore there is considerably material on them. In particular we quote here 3-loop results for the two-point correlator of the scalar and vector currents (keeping only terms with imaginary part). All expressions are for two flavors $N_f = 2$ and taken from [65] where one can find the original references:

$$\Pi_0^0(s) = -\frac{1}{(2\pi)^4} \frac{m_q^2}{8\pi^2} s \left\{ 6 \ln\left(-\frac{s}{\mu^2}\right) + \frac{\alpha_s}{\pi} \left[34 \ln\left(-\frac{s}{\mu^2}\right) - 6 \ln^2\left(-\frac{s}{\mu^2}\right) \right] + \left(\frac{\alpha_s}{\pi}\right)^2 \left[\left(\frac{10021}{24} - 109\zeta(3)\right) \ln\left(-\frac{s}{\mu^2}\right) - \frac{296}{3} \ln^2\left(-\frac{s}{\mu^2}\right) + \frac{53}{6} \ln^3\left(-\frac{s}{\mu^2}\right) \right] + O(\alpha_s^3) \right\}$$
(C.23)

and

$$\Pi_{1}^{1} = -\frac{1}{(2\pi)^{4}} \frac{s}{8\pi^{2}} \left\{ \ln\left(-\frac{s}{\mu^{2}}\right) + \frac{\alpha_{s}}{\pi} \ln\left(-\frac{s}{\mu^{2}}\right) + \left(\frac{\alpha_{s}}{\pi}\right)^{2} \left[\left(\frac{107}{8} - \frac{29\zeta(3)}{3}\right) \ln\left(-\frac{s}{\mu^{2}}\right) - \frac{29}{24} \ln^{2}\left(-\frac{s}{\mu^{2}}\right)\right] + O(\alpha_{s}^{3}) \right\}$$
(C.24)

In the previous expressions we only kept the parts that have a non-vanishing imaginary part because we are interested in $\rho = 2 \operatorname{Im}\Pi(s + i\epsilon)$ to find the finite energy sum rules (setting $m_{\pi} = 1$):

$$\frac{1}{s_0^{n+2}} \int_4^{s_0} \rho_0^0(x) x^n dx = \frac{m_q^2}{(2\pi)^4} \frac{3}{2\pi(n+2)} \left\{ 1 + \frac{\alpha_s}{\pi} \left[\frac{17}{3} + \frac{2}{n+2} \right] + \left(\frac{\alpha_s}{\pi} \right)^2 \left[\frac{10021}{144} - \frac{109}{6} \zeta(3) + \frac{296}{9(n+2)} + \frac{53}{6(n+2)^2} - \frac{53}{36} \pi^2 \right] + O(\alpha_s^3) \right\}$$
(C.25)

and

$$\frac{1}{s_0^{n+2}} \int_4^{s_0} \rho_1^1(x) x^n dx = \frac{1}{(2\pi)^4} \frac{1}{4\pi(n+2)} \left\{ 1 + \frac{\alpha_s}{\pi} + \left(\frac{\alpha_s}{\pi}\right)^2 \left[\left(\frac{107}{8} - \frac{29\zeta(3)}{3}\right) + \frac{29}{12(n+2)} \right] + O(\alpha_s^3) \right\}$$
(C.26)

Finally, for the S0 and P1 waves, we find useful to improve the procedure by using a different analytical kernel such as the one in [66] that captures more on the lower energy region ⁹:

$$K(s) = s^n \left(1 - \frac{s}{s_0}\right) e^{-s/s_0} \tag{C.27}$$

leading to the S0, P1 sum rules

$$\frac{1}{s_0^{n+2}} \int_4^{s_0} \rho_1^1(x) K(x) dx = m_q^2 \left\{ c_{n,0}^{S0} + c_{n,1}^{S0} \frac{\alpha_s}{\pi} + c_{n,2}^{S0} \left(\frac{\alpha_s}{\pi} \right)^2 + \mathcal{O}(\alpha_s^3) \right\} (C.28a)$$

$$\frac{1}{s_0^{n+2}} \int_4^{s_0} \rho_1^1(x) K(x) dx = c_{n,0}^{P1} + c_{n,1}^{P1} \frac{\alpha_s}{\pi} + c_{n,2}^{P1} \left(\frac{\alpha_s}{\pi} \right)^2 + \mathcal{O}(\alpha_s^3) \qquad (C.28b)$$

In the main text we use these "pinched" sum rules for ρ_0^0 , ρ_1^1 up to n=6. The corresponding numerical coefficients $c_{i,j}$ are shown in tables 5, 6 for reference.

⁹as compared with the weight s^n that tends to favor the larger values of x close to s_0

$i \backslash j$	0	1	2
0	3.1750×10^{-5}	2.4104×10^{-4}	2.2490×10^{-3}
1	1.4299×10^{-5}	1.0012×10^{-4}	8.3028×10^{-4}
2	7.9936×10^{-6}	5.3436×10^{-5}	4.1288×10^{-4}
3	5.0653×10^{-6}	3.2859×10^{-5}	2.4218×10^{-4}
4	3.4828×10^{-6}	2.2124×10^{-5}	1.5766×10^{-4}
5	2.5359×10^{-6}	1.5862×10^{-5}	1.1022×10^{-4}

Table 5: Numerical values of the S0 sum rule coefficients $c_{i,j}^{S0}$.

$i \backslash j$	0	1	2
-1	1.8783×10^{-5}	1.8783×10^{-5}	1.1097×10^{-4}
0	5.2916×10^{-6}	5.2916×10^{-6}	2.1597×10^{-5}
1	2.3831×10^{-6}	2.3831×10^{-6}	8.0286×10^{-6}
2	1.3323×10^{-6}	1.3323×10^{-6}	3.9775×10^{-6}
3	8.4421×10^{-7}	8.4421×10^{-7}	2.3186×10^{-6}
4	5.8047×10^{-7}	5.8047×10^{-7}	1.4997×10^{-6}

Table 6: Numerical values of the P1 sum rule coefficients $c_{i,j}^{P1}$.

References

- Y. He and M. Kruczenski, "Gauge theory bootstrap," Phys. Rev. Lett. 133 (Nov, 2024) 191601.
 https://link.aps.org/doi/10.1103/PhysRevLett.133.191601.
- [2] Y. He and M. Kruczenski, "Bootstrapping gauge theories," Phys. Rev. D 110 (Nov, 2024) 096001. https://link.aps.org/doi/10.1103/PhysRevD.110.096001.
- [3] Y. He and M. Kruczenski, "Gauge Theory Bootstrap: Pion amplitudes and low energy parameters," arXiv:2403.10772 [hep-th].
- [4] G. Colangelo, J. Gasser, and H. Leutwyler, " $\pi\pi$ scattering," Nucl. Phys. B **603** (2001) 125–179, arXiv:hep-ph/0103088.
- [5] J. R. Pelaez and F. J. Yndurain, "The Pion-pion scattering amplitude," *Phys. Rev. D* 71 (2005) 074016, arXiv:hep-ph/0411334.
- [6] J. Bijnens, G. Colangelo, and J. Gasser, "K(l4) decays beyond one loop," Nucl. Phys. B 427 (1994) 427–454, arXiv:hep-ph/9403390.

- [7] J. Bijnens, G. Colangelo, G. Ecker, J. Gasser, and M. E. Sainio, "Pion-pion scattering at low energy," *Nucl. Phys. B* **508** (1997) 263–310, arXiv:hep-ph/9707291.
- [8] J. Bijnens, G. Colangelo, and P. Talavera, "The Vector and scalar form-factors of the pion to two loops," *JHEP* **05** (1998) 014, arXiv:hep-ph/9805389.
- [9] B. Ananthanarayan, I. Caprini, G. Colangelo, J. Gasser, and H. Leutwyler, "Scalar form factors of light mesons," *Physics Letters B* **602** no. 3-4, (Nov, 2004) 218–225.
- [10] A. Guerrieri, K. Häring, and N. Su, "From data to the analytic S-matrix: A Bootstrap fit of the pion scattering amplitude," arXiv:2410.23333 [hep-th].
- [11] J. R. Peláez, P. Rabán, and J. R. de Elvira, "Global parametrizations of $\pi\pi$ scattering with dispersive constraints: Beyond the S0 wave," *Phys. Rev. D* **111** no. 7, (2025) 074003, arXiv:2412.15327 [hep-ph].
- [12] Flavour Lattice Averaging Group (FLAG) Collaboration, Y. Aoki et al., "FLAG Review 2024," arXiv:2411.04268 [hep-lat].
- [13] R. J. Eden, P. V. Landshoff, D. I. Olive, and J. C. Polkinghorne, *The analytic S-matrix*. Cambridge Univ. Press, Cambridge, 1966.
- [14] G. Chew, The Analytic S Matrix: A Basis for Nuclear Democracy. W. A. Benjamin, 1966. https://books.google.fr/books?id=yPNBAAAAIAAJ.
- [15] F. Zachariasen, "Self-consistent calculation of the mass and width of the j=1, t=1, $\pi\pi$ resonance," *Phys. Rev. Lett.* **7** (Aug, 1961) 112–113. https://link.aps.org/doi/10.1103/PhysRevLett.7.112.
- [16] P. D. B. Collins, "Inadequacies of the new form of the strip approximation for the $\pi-\pi$ scattering amplitude," *Phys. Rev.* **142** (Feb, 1966) 1163–1172. https://link.aps.org/doi/10.1103/PhysRev.142.1163.
- [17] M. F. Paulos, J. Penedones, J. Toledo, B. C. van Rees, and P. Vieira, "The S-matrix bootstrap. Part I: QFT in AdS," JHEP 11 (2017) 133, arXiv:1607.06109 [hep-th].
- [18] M. F. Paulos, J. Penedones, J. Toledo, B. C. van Rees, and P. Vieira, "The S-matrix bootstrap II: two dimensional amplitudes," *JHEP* 11 (2017) 143, arXiv:1607.06110 [hep-th].

- [19] M. F. Paulos, J. Penedones, J. Toledo, B. C. van Rees, and P. Vieira, "The S-matrix bootstrap. Part III: higher dimensional amplitudes," *JHEP* 12 (2019) 040, arXiv:1708.06765 [hep-th].
- [20] M. Kruczenski, J. Penedones, and B. C. van Rees, "Snowmass White Paper: S-matrix Bootstrap," arXiv:2203.02421 [hep-th].
- [21] A. L. Guerrieri, J. Penedones, and P. Vieira, "Bootstrapping QCD Using Pion Scattering Amplitudes," *Phys. Rev. Lett.* **122** no. 24, (2019) 241604, arXiv:1810.12849 [hep-th].
- [22] A. Bose, A. Sinha, and S. S. Tiwari, "Selection rules for the S-Matrix bootstrap," arXiv:2011.07944 [hep-th].
- [23] A. Bose, P. Haldar, A. Sinha, P. Sinha, and S. S. Tiwari, "Relative entropy in scattering and the S-matrix bootstrap," *SciPost Phys.* **9** (2020) 081, arXiv:2006.12213 [hep-th].
- [24] A. Guerrieri, J. Penedones, and P. Vieira, "S-matrix Bootstrap for Effective Field Theories: Massless Pions," arXiv:2011.02802 [hep-th].
- [25] C. Fernandez, A. Pomarol, F. Riva, and F. Sciotti, "Cornering large-N_c QCD with positivity bounds," *JHEP* **06** (2023) 094, arXiv:2211.12488 [hep-th].
- [26] J. Albert and L. Rastelli, "Bootstrapping pions at large N," JHEP 08 (2022) 151, arXiv:2203.11950 [hep-th].
- [27] J. Albert, J. Henriksson, L. Rastelli, and A. Vichi, "Bootstrapping mesons at large N: Regge trajectory from spin-two maximization," arXiv:2312.15013 [hep-th].
- [28] J. Albert and L. Rastelli, "Bootstrapping Pions at Large N. Part II: Background Gauge Fields and the Chiral Anomaly," arXiv:2307.01246 [hep-th].
- [29] D. Karateev, S. Kuhn, and J. a. Penedones, "Bootstrapping Massive Quantum Field Theories," *JHEP* **07** (2020) 035, arXiv:1912.08940 [hep-th].
- [30] D. Karateev, "Two-point functions and bootstrap applications in quantum field theories," *JHEP* **02** (2022) 186, arXiv:2012.08538 [hep-th].

- [31] H. Chen, A. L. Fitzpatrick, and D. Karateev, "Bootstrapping 2d ϕ^4 theory with Hamiltonian truncation data," *JHEP* **02** (2022) 146, arXiv:2107.10286 [hep-th].
- [32] M. Correia, J. Penedones, and A. Vuignier, "Injecting the UV into the bootstrap: Ising Field Theory," *JHEP* **08** (2023) 108, arXiv:2212.03917 [hep-th].
- [33] L. Cordova, M. Correia, A. Georgoudis, and A. Vuignier, "The O(N) monolith reloaded: sum rules and Form Factor Bootstrap," *JHEP* 01 (2024) 093, arXiv:2311.03031 [hep-th].
- [34] A. Zahed, "Bootstrapping leading hadronic muon anomaly," arXiv:2412.00187 [hep-th].
- [35] G. Peter Lepage and S. J. Brodsky, "Exclusive processes in quantum chromodynamics: Evolution equations for hadronic wavefunctions and the form factors of mesons," *Physics Letters B* **87** no. 4, (11, 1979) .
- [36] R. Cordoba to appear.
- [37] M. Shifman, A. Vainshtein, and V. Zakharov, "Qcd and resonance physics. theoretical foundations," *Nuclear Physics B* **147** no. 5, (1979) 385–447.
- [38] M. Shifman, A. Vainshtein, and V. Zakharov, "Qcd and resonance physics. applications," *Nuclear Physics B* **147** no. 5, (1979) 448–518.
- [39] M. A. Shifman, A. I. Vainshtein, and V. I. Zakharov, "QCD and Resonance Physics. The rho-omega Mixing," *Nucl. Phys. B* **147** (1979) 519–534.
- [40] J. Gasser, "Chiral perturbation theory and effective lagrangians," *Nuclear Physics B* **279** no. 1, (1987) 65–79.
- [41] Y. He, A. Irrgang, and M. Kruczenski, "A note on the S-matrix bootstrap for the 2d O(N) bosonic model," JHEP 11 (2018) 093, arXiv:1805.02812 [hep-th].
- [42] P. Tourkine and A. Zhiboedov, "Scattering from production in 2d," *JHEP* **07** (2021) 228, arXiv:2101.05211 [hep-th].
- [43] P. Tourkine and A. Zhiboedov, "Scattering amplitudes from dispersive iterations of unitarity," *JHEP* 11 (2023) 005, arXiv:2303.08839 [hep-th].

- [44] X.-B. Tong, J.-P. Ma, and F. Yuan, "Gluon gravitational form factors at large momentum transfer," *Physics Letters B* **823** (Dec., 2021) 136751.
- [45] X.-B. Tong, J.-P. Ma, and F. Yuan, "Perturbative calculations of gravitational form factors at large momentum transfer," *Journal of High Energy Physics* **2022** no. 10, (Oct., 2022) .
- [46] L. Chang, I. C. Cloët, C. D. Roberts, S. M. Schmidt, and P. C. Tandy, "Pion electromagnetic form factor at spacelike momenta," *Phys. Rev. Lett.* 111 (Oct, 2013) 141802. https://link.aps.org/doi/10.1103/PhysRevLett.111.141802.
- [47] C. Lopez and G. Mennessier, "Bounds on the pi0 pi0 Amplitude," Nucl. Phys. B 118 (1977) 426–444.
- [48] Y. He and M. Kruczenski, "S-matrix bootstrap in 3+1 dimensions: regularization and dual convex problem," *JHEP* **08** (2021) 125, arXiv:2103.11484 [hep-th].
- [49] A. Guerrieri and A. Sever, "Rigorous Bounds on the Analytic S Matrix," *Phys. Rev. Lett.* **127** no. 25, (2021) 251601, arXiv:2106.10257 [hep-th].
- [50] H. Chen, A. L. Fitzpatrick, and D. Karateev, "Nonperturbative bounds on scattering of massive scalar particles in d ≥ 2," JHEP 12 (2022) 092, arXiv:2207.12448 [hep-th].
- [51] J. Elias Miro, A. Guerrieri, and M. A. Gumus, "Bridging positivity and S-matrix bootstrap bounds," *JHEP* **05** (2023) 001, arXiv:2210.01502 [hep-th].
- [52] S. D. Protopopescu, M. Alston-Garnjost, A. Barbaro-Galtieri, S. M. Flatte, J. H. Friedman, T. A. Lasinski, G. R. Lynch, M. S. Rabin, and F. T. Solmitz, "Pi pi Partial Wave Analysis from Reactions pi+ p —> pi+ pi- Delta++ and pi+ p —> K+ K- Delta++ at 7.1-GeV/c," Phys. Rev. D 7 (1973) 1279.
- [53] M. Losty, V.Chaloupka, A.Ferrando, L.Montanet, E.Paul;, D.Yaffe, A.Zieminski, J.Alitti, B.Gandois, and J.Louie., "A study of $\pi\pi$ scattering from πp interactions at 3.93 gev/c," Nuclear Physics B **69** (1974) 185–204.
- [54] B. Hyams *et al.*, "A Study of All the pi pi Phase Shift Solutions in the Mass Region 1.0-GeV to 1.8-GeV from pi- p \rightarrow pi- pi+ n at 17.2-GeV," *Nucl. Phys. B* **100** (1975) 205–224.

- [55] J. Gasser and H. Leutwyler, "Chiral perturbation theory to one loop," *Annals of Physics* **158** no. 1, (1984) 142–210.
- [56] **Particle Data Group** Collaboration, R. L. Workman and Others, "Review of Particle Physics," *PTEP* **2022** (2022) 083C01.
- [57] S. Weinberg, "Pion scattering lengths," Phys. Rev. Lett. 17 (1966) 616–621.
- [58] J. R. Pelaez, "From controversy to precision on the sigma meson: a review on the status of the non-ordinary $f_0(500)$ resonance," *Phys. Rept.* **658** (2016) 1, arXiv:1510.00653 [hep-ph].
- [59] B. Pire, "Exclusive reactions in QCD," in Les Houches Summer School on Theoretical Physics, Session 66: Trends in Nuclear Physics, 100 Years Later, pp. 567–591. 7, 1996. arXiv:nucl-th/9612009.
- [60] K. Huang, Statistical Mechanics. John Wiley and Sons, Inc., 1987.
- [61] R. Dashen, S.-k. Ma, and H. J. Bernstein, "s-matrix formulation of statistical mechanics," Phys. Rev. 187 (Nov, 1969) 345-370. https://link.aps.org/doi/10.1103/PhysRev.187.345.
- [62] R. Venugopalan and M. Prakash, "Thermal properties of interacting hadrons," Nuclear Physics A 546 no. 4, (1992) 718-760. https: //www.sciencedirect.com/science/article/pii/0375947492900055.
- [63] P. Baratella, J. E. Miro, and E. Gendy, "Thermodynamics from the s-matrix reloaded, with applications to qcd and the confining flux tube," 2024. https://arxiv.org/abs/2408.06729.
- [64] **STAR** Collaboration, M. S. Abdallah *et al.*, "Pair invariant mass to isolate background in the search for the chiral magnetic effect in Au + Au collisions at sNN=200 GeV," *Phys. Rev. C* **106** no. 3, (2022) 034908, arXiv:2006.05035 [nucl-ex].
- [65] S. Narison, QCD as a Theory of Hadrons: From Partons to Confinement. Cambridge Monographs on Particle Physics, Nuclear Physics and Cosmology. Cambridge University Press, 2004.
- [66] S. N. Cherry and M. R. Pennington, "Qcd finite energy sum rules and the isoscalar scalar mesons," 2001.